Supporting Information for

Serendipity of Topological Nontrivial Band Gap in 2D Borophene Subunit Lattice with Mirror Symmetry Broken

Aizhu Wang[1,2]*, Lei Shen[3], Mingwen Zhao[4]*, Xiaoming Zhang[4], Tao He[4], Weifeng Li[4], Yuanping Feng[5]*, and Hong Liu[1,6]*

[1]*Institute for Advanced Interdisciplinary Research, University of Jinan, Jinan, Shandong, 250022, China*

[2]*Department of Electrical and Computer Engineering and Department of Physics, National University of Singapore, Singapore, 117579, Singapore*

[3]*Department of Mechanical Engineering, Engineering Science Programme, Faculty of Engineering, National University of Singapore, Singapore, 117575, Singapore*

[4]*School of Physics and State Key Laboratory of Crystal Materials, Shandong University, Jinan Shandong, 250100, China*

[5]*Department of Physics & Centre for Advanced Two-dimensional Materials, National University of Singapore, Singapore, 117542, Singapore*

[6]*State Key Laboratory of Crystal Materials, Shandong University, Jinan, Shandong, 250100, China*

*Corresponding authors:

A. W.: E-mail: ifc_wangaz@ujn.edu.cn

M. Z.: E-mail: zmw@sdu.edu.cn

Y. F.: E-mail: phyfyp@nus.edu.sg

H. L.: E-mail: hongliu@sdu.edu.cn

POSCAR of WB_4 with mirror symmetry

1.0

2.9640769958 0.0000000000 0.0000000000

-1.4820384979 2.5669659772 0.0000000000

0.0000000000 0.0000000000 17.8898410797

B W

4 1

Direct

0.666666687 0.333333343 0.407867491

0.333333343 0.666666687 0.407867491

0.666666687 0.333333343 0.592132509

0.333333343 0.666666687 0.592132509

0.000000000 0.000000000 0.500000000

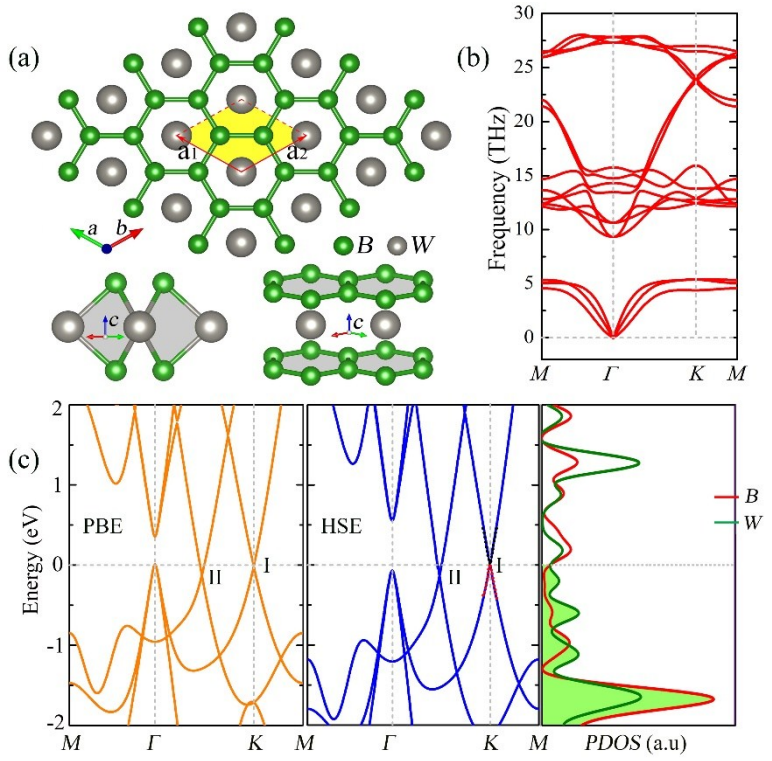

Figure S1 The schematic illustration (a), phonon spectrum (b) and electronic structures (c) of WB_4 with mirror symmetry. The unit cell is indicated by the red line. The red and black dots represent the Dirac band of cone I reproduced by TB model. The energy at the Fermi level was set to zero.

In the absence of spin-orbit coupling (SOC), the mirror symmetry protects WB_4 lattice to spawn multiple Dirac bands around the Fermi level with high velocities. We also take the Dirac cone I as an example and adopt the tight-binding (TB) method to reproduce the electronic bands in the vicinity of the Fermi level and in an attempt to gain more insight into the existence of Dirac cones. The TB Hamiltonian reads as follows:

$$H = \varepsilon \sum_{i\alpha} c_{i\alpha}^{+} c_{i\alpha} + \sum_{\langle i,j\rangle \alpha,\beta} t_{i,j,\alpha,\beta} c_{i\alpha}^{+} c_{j\beta}$$

here, α, $\beta \in p_z, d_{xz}, d_{yz}$, where ε is the on-sit energy of different orbitals, and $c_{i\alpha}^{+}$ and $c_{i\alpha}$ are the creation and annihilation operators of an α-orbital electron at the i-th atom, respectively. The optimal values for the mirror symmetry WB_4 lattice are $\varepsilon_{z,z}$ = -6.76, $\varepsilon_{xz,xz}$ = -1.62, $\varepsilon_{yz,yz}$ = -1.23, $t_{z,xz}$ = 0.61, $t_{z,yz}$ = 1.45, $t_{xz,yz}$ = -0.01, respectively. With the above parameters, our TB Hamiltonian reproduces well the two Dirac band of the WB_4 lattice given by DFT calculations, as shown in **Figure S1**. By the same strategy, we can reproduce the Dirac bands for cone II, which contain the coupling between p orbitals of B and the $d_{z2}/d_{x2-y2}/d_{xy}$ orbitals of W. A slight deviation of the TB model to the DFT data can be attributed to the small contribution of the s orbital of B and W together with the p orbital of W, which are omitted in this TB Hamiltonian.

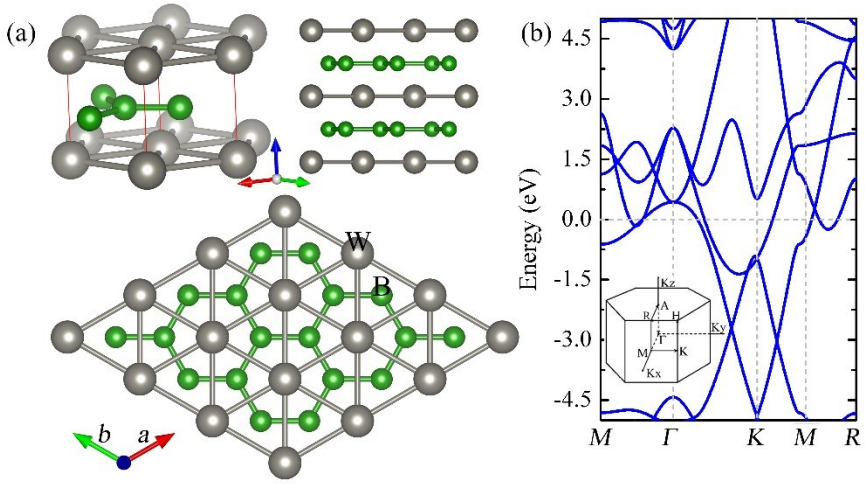

Figure S2 (a) Schematic illustration of fabrication of WB_2 (P6/mmm, number 191) crystal. The unit cell is indicated by the red line. (b) The calculated band structures based on PBE calculations were also listed here. The energy at the Fermi level was set to zero.

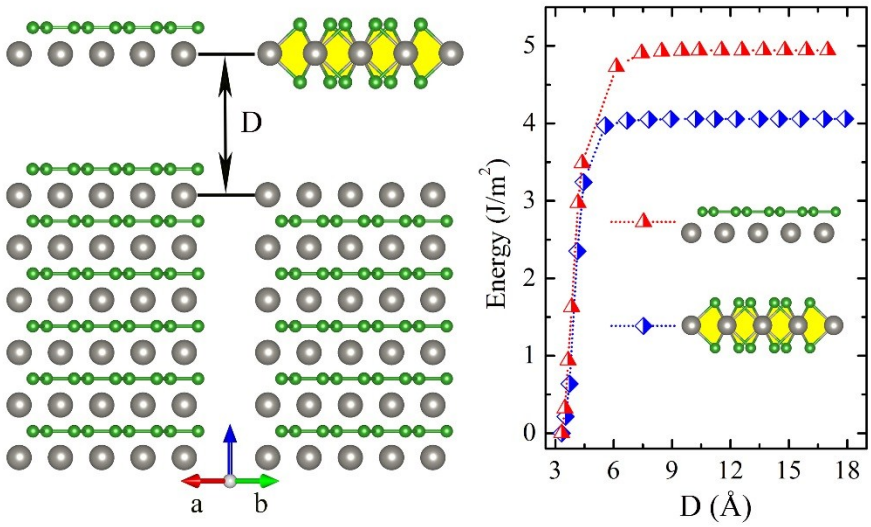

Figure S3 (a) Schematic representation of the exfoliation process of WB_2 monolayer and WB_4 monolayer. (b) Energy increase *E* as a function of interlayer distance (D).

The cleavage energy E_{cl} is defined as the minimum energy required to exfoliate a monolayer from bulk. We used a seven-slab model to mimic a bulk material and calculated the energy increase as a WB_4 monolayer is exfoliated from the slab. A vacuum layer at least 15 Å was incorporated into the seven-layer slab to avoid the artificial interaction between two neighboring slabs. **Figure S3** gives the variation of energy (and its derivative) as a function of the interlayer distance (D) between the top most monolayer and the remnant layers, which was fixed during the exfoliation process. The calculated cleavage energy E_{cl} of WB_4 is about 4.06 J m^{-2}. The cleavage strength (χ) was further obtained from the derivative of energy with respect to the distance, which is about 2.66 GPa. It is noteworthy that the calculated cleavage energy of WB_4 is smaller than that of WB_2 suggesting high plausibility to extract the WB_4 monolayer from the bulk in experiments.

The POSCAR of WB_4 with mirror symmetry broken

POSCAR of WB_4 with mirror symmetry broken

1.00000000000000

2.9549929247882769 -0.0000006174470997 0.0000000000000000

-1.4774969972983534 2.5590986327995213 0.0000000000000000

0.0000000000000000 0.0000000000000000 18.0000000000000000

B W

4 1

Direct

0.6666664480069642 0.3333326765044902 0.4981008572670902

0.3333326772188414 0.6666664472412336 0.4981008572992636

0.6666664514929224 0.3333326968645238 0.6811141708041220

0.3333326980226943 0.6666664515805962 0.6811141709144835

0.0000017471373042 0.0000017462104296 0.5896587139821321

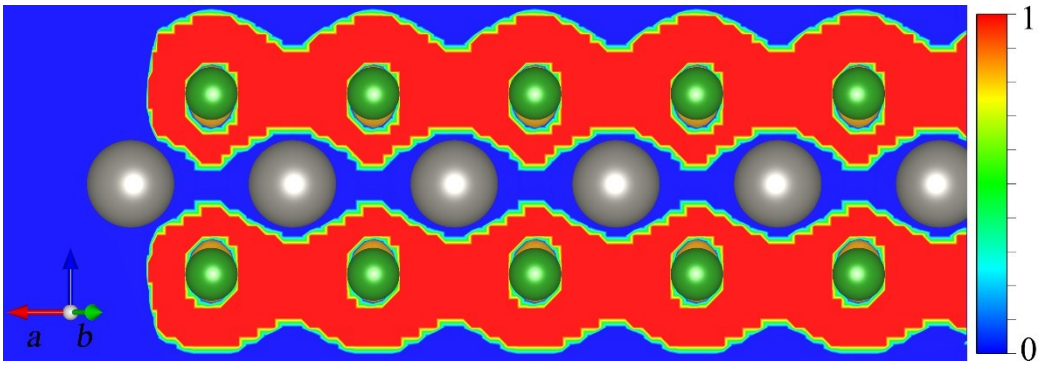

Figure S4 (Color online). The electron localization function (ELF) profiles on the plane perpendicular to the basal plane of the monolayers with an isovalue of 0.4 $Å^{-3}$

The structure of WB_4 can be viewed as an interconnected, sandwich-like configuration comprising W framework-inserted borophene subunits. The electron localization function (ELF) profile of the WB_4 monolayer indicates that B atoms are chemically bonded to the triangle W lattice, while the covalent like B-B bonds are preserved, as shown in Figure S3. Obviously, the metal bonds have longer bond lengths so that metallic like W-B bonds are weaker, meanwhile, electron density redistribution takes place around W and B atoms, which facilitates the protection of semimetal phase of the WB_4 framework.

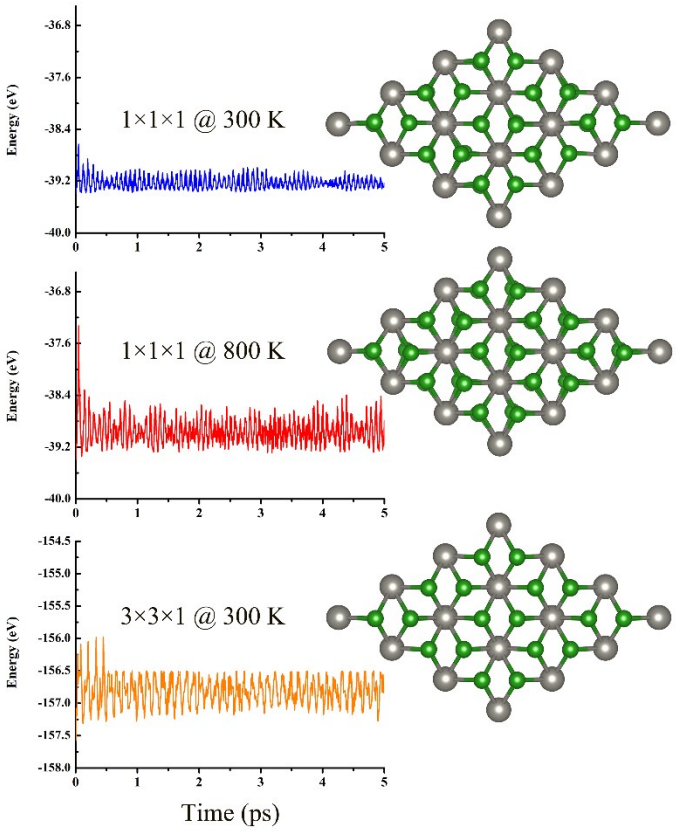

Figure S5 (Color online). The fluctuations of energy (with different models) as functions of the molecular dynamic (MD) simulation step at 300 K and 800 K.

Our MD simulations clearly indicate that geometry of WB_4 remains unchanged in addition to small fluctuations of the temperature and the total energy with the passage of time. Although the time scale is short, our MD results imply that the WB_4 framework is stable at room temperature (300 K), but no longer unstable at high temperature (800 K).

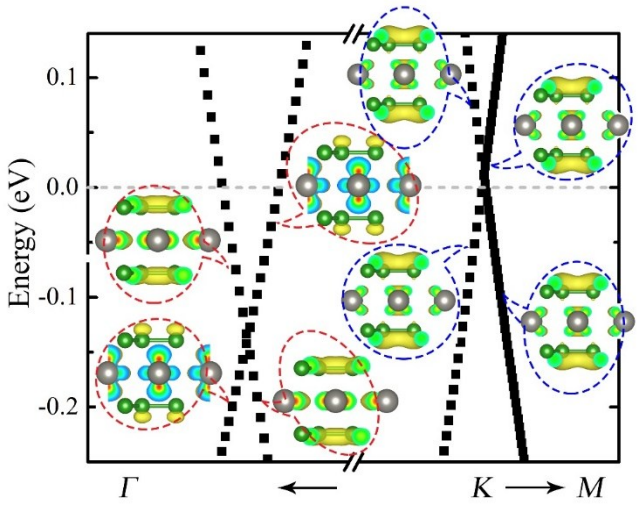

Figure S6 Charge density distributions near the Fermi level, both Dirac cone (cone I and cone II) are from *d* orbitals of W and *p* orbitals of B atoms. Cone I is isotropic with a high symmetry, while, cone II is anisotropic with a lower symmetry. The energy at the Fermi level was set to zero.

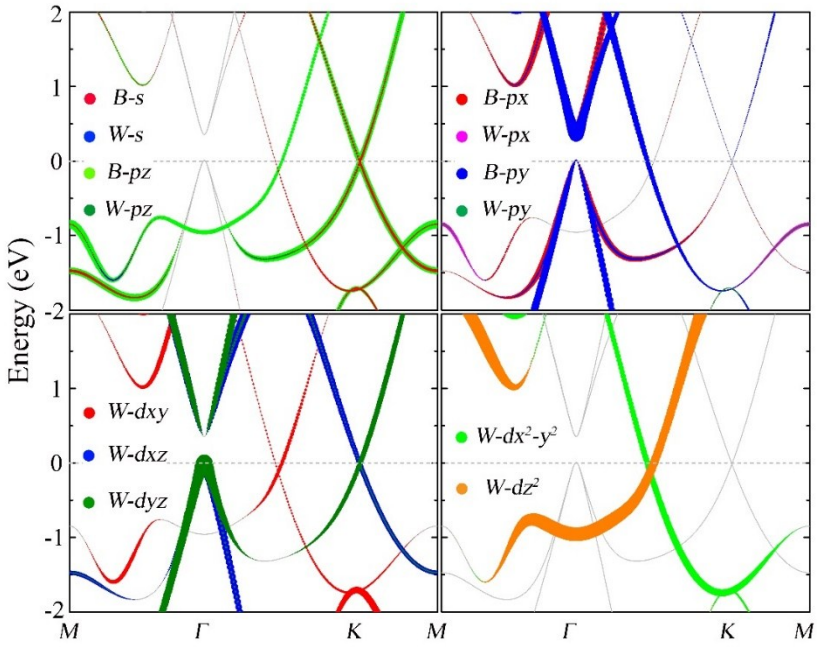

Figure S7 Orbital-resolved band structures without SOC around Fermi level based on PBE calculations. The size of colorful dots is proportion to the contribution of the different orbitals on the wave function. The energy at the Fermi level was set to zero.

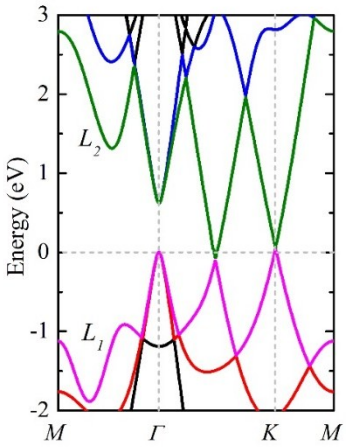

Figure S8 Electronic band lines (without SOC) of WB_4 in proximity of the Fermi level along the high symmetric points in BZ based on HSE06 function. The energy at the Fermi level was set to zero. L_1 (purple line) and L_2 (green line) represent the valence band maximum and conductor band minimum, respectively.

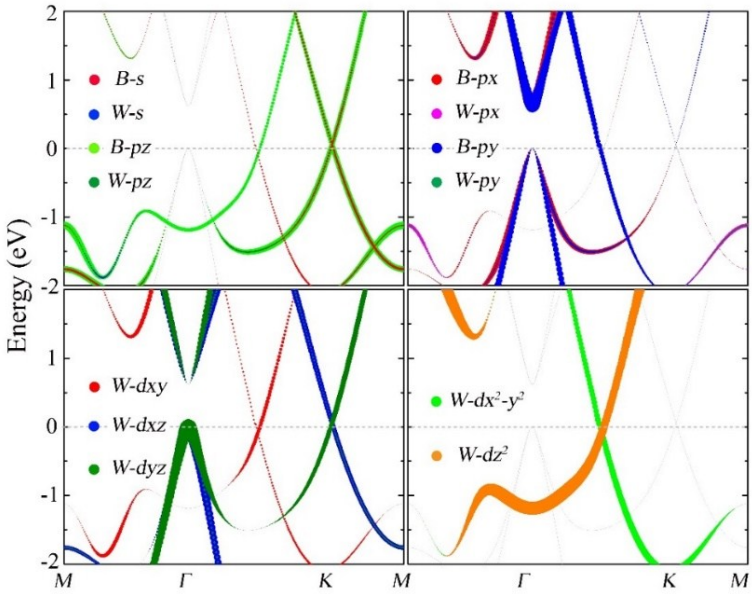

Figure S9 Orbital-resolved band structures without SOC around Fermi level based on HSE06 calculations. The size of colorful dots is proportion to the contribution of the different orbitals on the wave function. The energy at the Fermi level was set to zero.

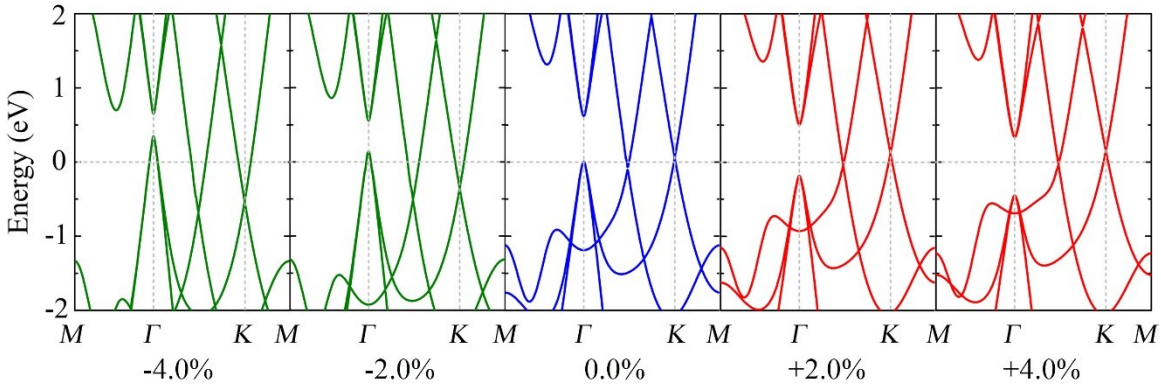

Figure S10 (Color online) Electronic band structure evolution of 2D WB_4 lattice with external strain along the *xy*-direction based on HSE06 function. The energy at the Fermi level is set to zero.

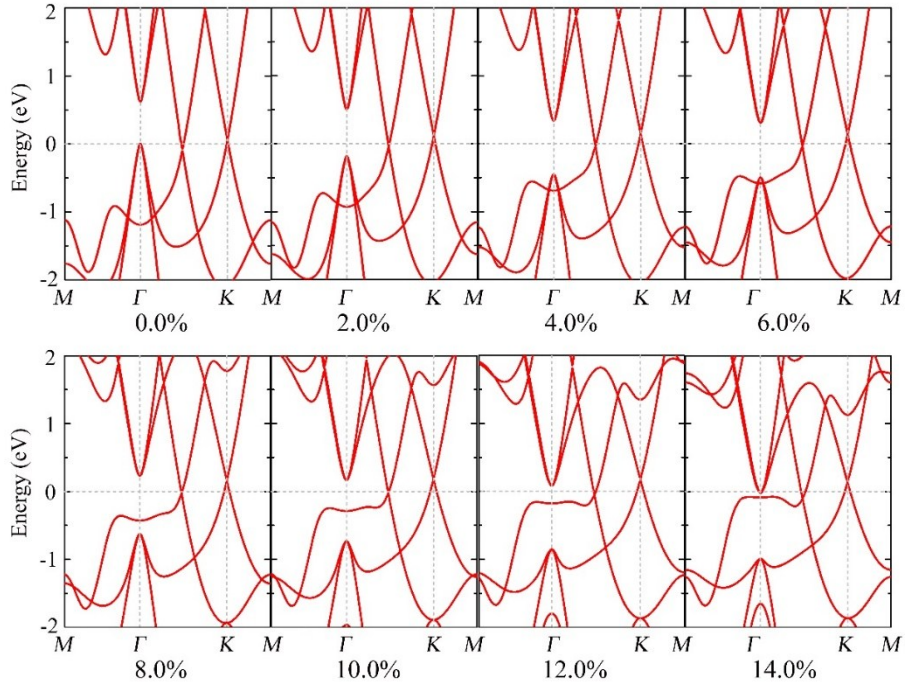

Figure S11 Band structure evolutions of the 2D WB_4 lattice with external stretching strain along the *xy*-direction based on HSE06 functional. The energy at the Fermi level was set to zero.

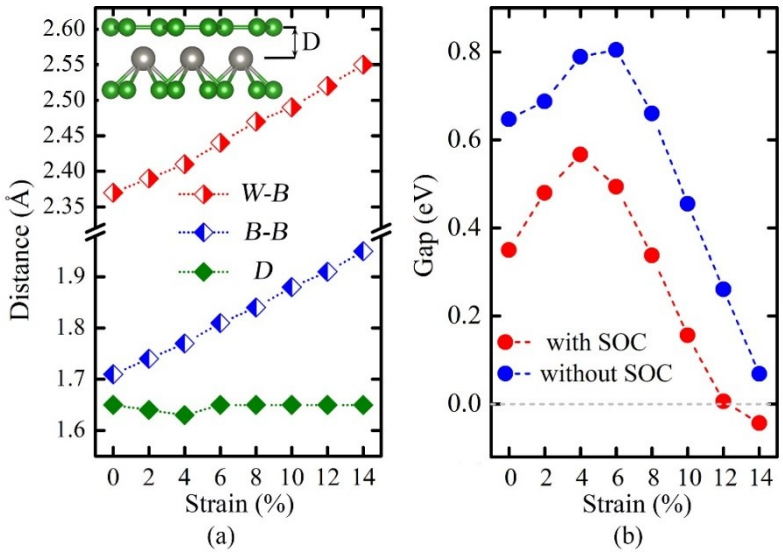

Figure S12 The evolutions of bonds (a) and band gaps (with and without SOC) of gamma point (b). The negative band gap in (b) represents the band inversion.

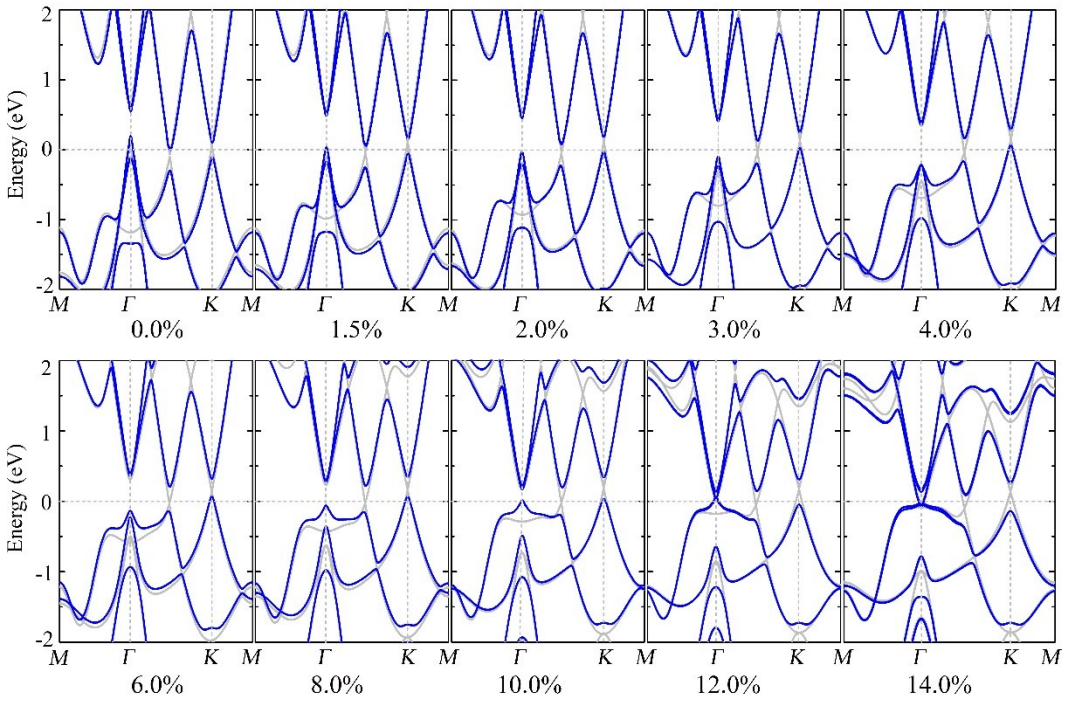

Figure S13 the SOC band structure evolutions of the 2D WB_4 lattice with external stretching strain along the *xy*-direction based on HSE06 functional. The energy at the Fermi level was set to zero.

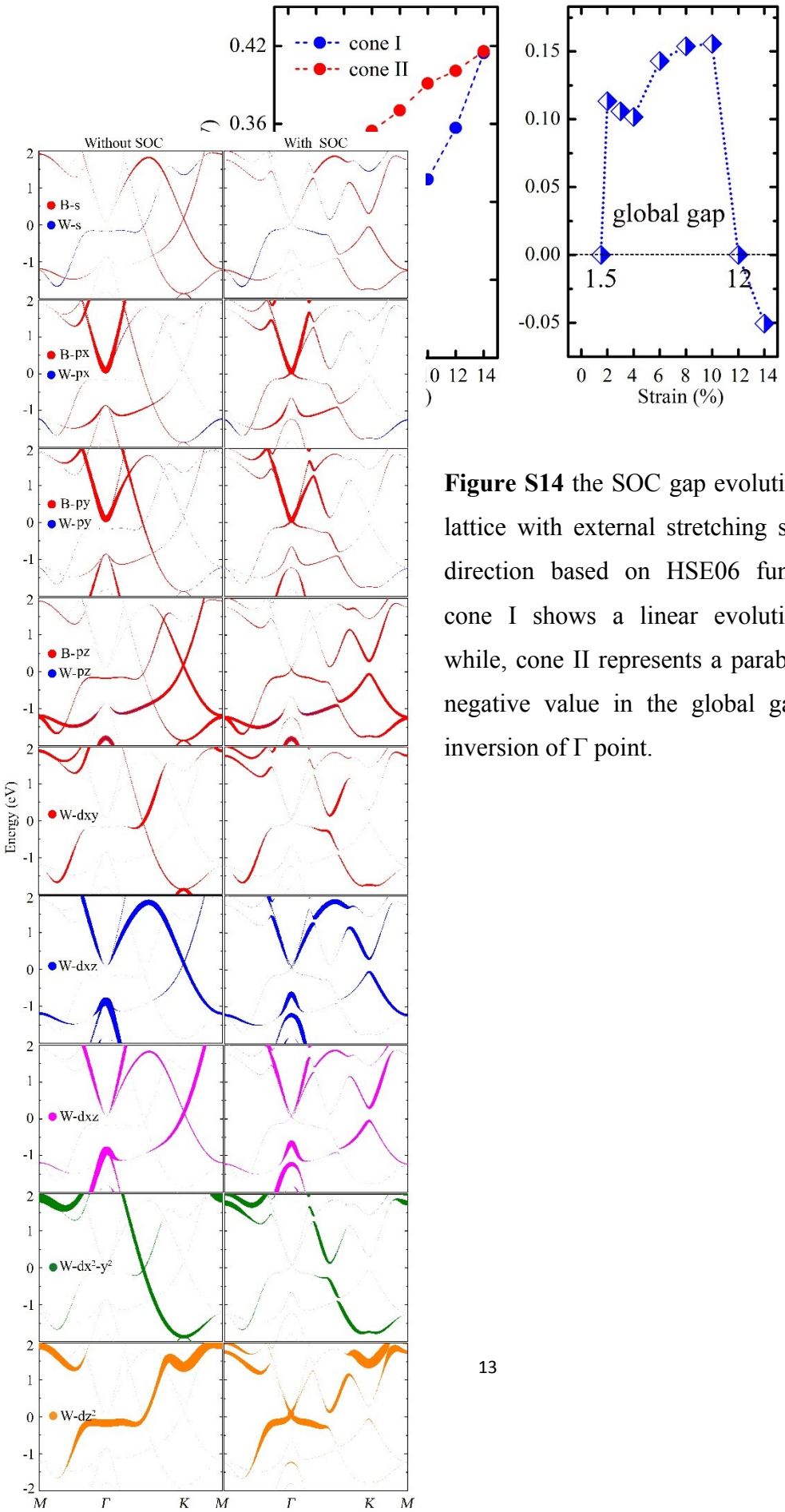

Figure S14 the SOC gap evolutions of the 2D WB_4 lattice with external stretching strain along the *xy*-direction based on HSE06 functional. Typically, cone I shows a linear evolutionary relationship, while, cone II represents a parabolic evolution. The negative value in the global gap represents band inversion of Γ point.

Figure S15 Orbital-resolved band structures under the strain of 12% with and without SOC around Fermi level based on HSE06 calculations. The size of colorful dots is proportion to the contribution of the different orbitals on the wave function. The energy at the Fermi level was set to zero.

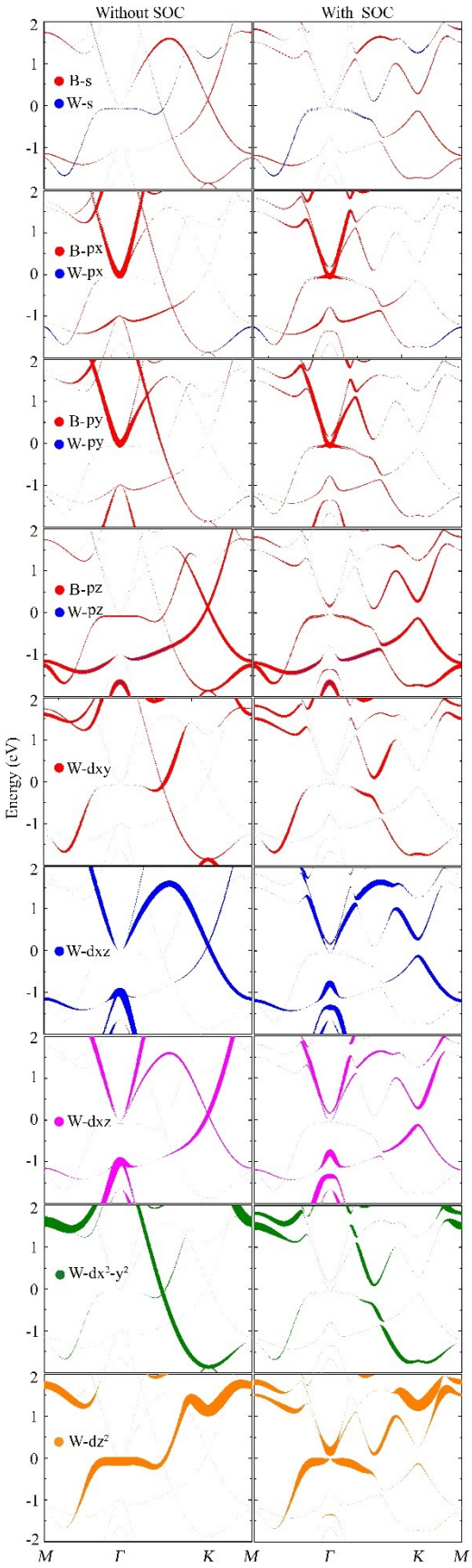

Figure S16 Orbital-resolved band structures under the strain of 14% with and without SOC around Fermi level based on HSE06 calculations. The size of colorful dots is proportion to the contribution of the different orbitals on the wave function. The energy at the Fermi level was set to zero.

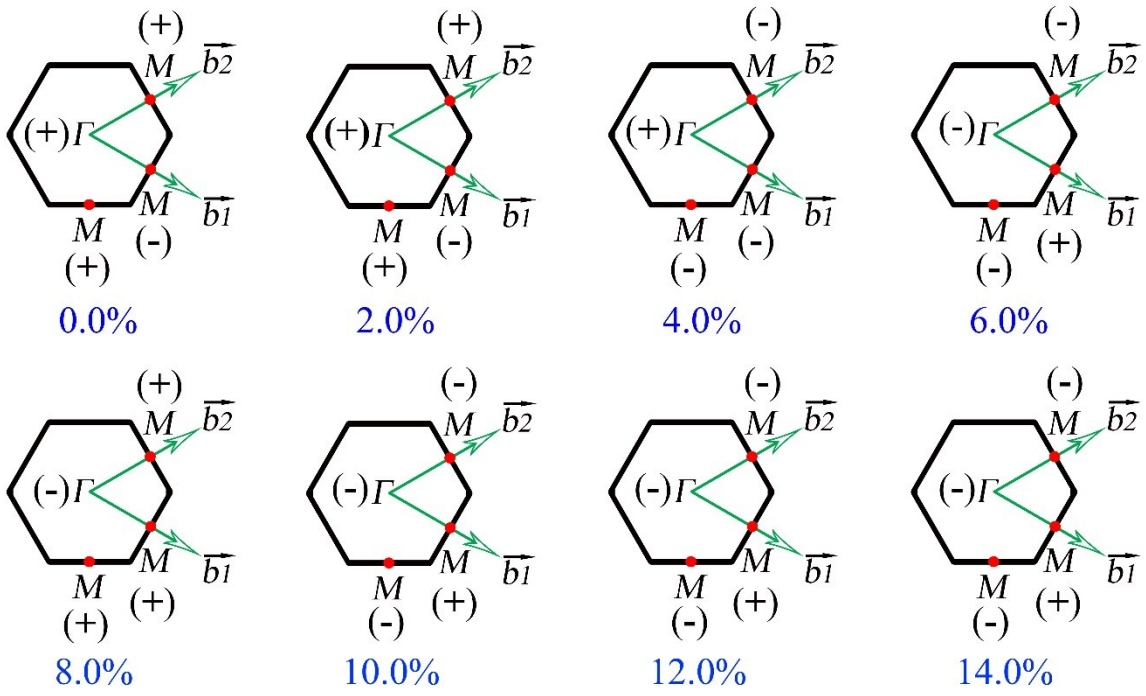

Figure S17 The corresponding BZ with the values of δ_i associated with the time reversal invariant momenta of SOC gaps is shown. The basis vectors of the reciprocal lattice are indicated by $\mathbf{b_1}$ and $\mathbf{b_2}$.

Here, the parity criteria proposed by Fu and Kane was adopted to determine topological feature of WB_4 lattice based on the calculation of Z_2 topological index. Here, the Z_2 index is determined by the parity of occupied bands on each time-reversal invariant momentum. In their strategy, the Z_2 invariant v is defined by

$$(-1)^{v} = \prod_{i} \delta_i \quad \text{with} \quad \delta_i = \prod_{m=1}^{N} \xi_{2m}(\Gamma_i)$$

for 2N occupied bands. $\xi_{2\mathrm{m}}(\Gamma_i) = \pm 1$ is the parity eigenvalue of the $2m$-th occupied energy band at the time-reversal invariant momentum Γ_{i}. The two states of a Kramers doublet have the same parity, $\xi_{2\mathrm{m}} = \xi_{2m-1}$. It means that with inversion symmetry, the Z_2 topological invariants can be deduced from the knowledge of the parity of the four time-reversal and parity invariant points at BZ. This provides a simple method for determining the topological phases of the lattice

inversion symmetry, without having to know about the global properties of the energy bands. For the WB_4 lattice, the four time-reversal invariant momenta occur at $\Gamma_{i=(n_1,n_2)} = (n_1 \vec{b}_1 + n_2 \vec{b}_2)/2$ with n_1, n_2 = 0, 1 and $\vec{b}_1$, $\vec{b}_2$ are primitive reciprocal lattice vectors, which correspond to the *Γ* and three *M* points in BZ.

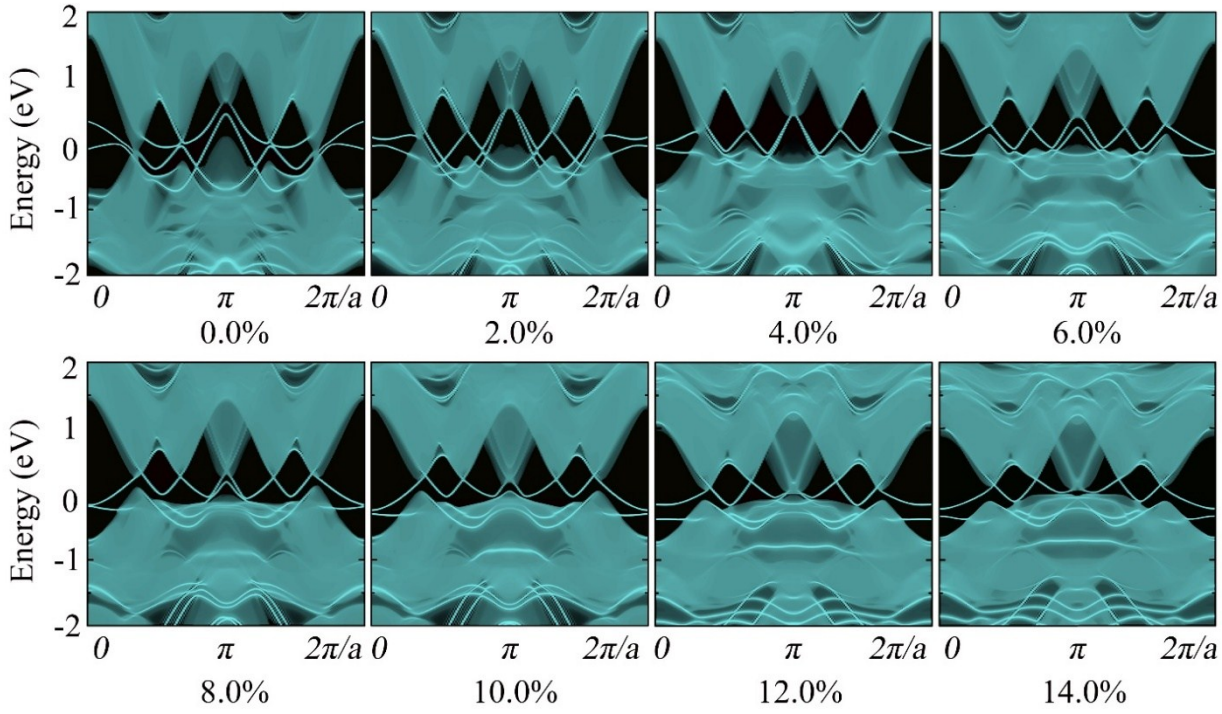

Figure S18 Semi-infinite edge states variation based on MLWFs. The energy at the Fermi level was set to zero.